THE JOURNAL OF PHYSICAL CHEMISTRY C

pubs.acs.org/JPCC Article

Disperse Multimetal Atom-Doped Carbon as Efficient Bifunctional Electrocatalysts for Oxygen Reduction and Evolution Reactions: Design Strategies

Detao Zhang, Lele Gong, Jun Ma, Xiaowei Wang, Lipeng Zhang,* and Zhenhai Xia*

Cite This: J. Phys. Chem. C 2020, 124, 27387−27395 Read Online

ACCESS | Metrics & More | Article Recommendations | Supporting Information

ABSTRACT: Disperse metal atoms can boost the catalytic activities of carbon-based electrocatalysts for various important chemical reactions at the heart of clean energy conversion technologies, such as oxygen reduction reaction (ORR) or oxygen evolution reaction (OER), but there lacks fundamental understanding and design principle of the catalysts. Herein, we design new disperse metal atom catalysts with single-, dual-, and tri-metal sites coordinated by nitrogen and study their catalytic activities by using the density functional theory methods. The electronic structures, reaction free energies, reaction pathways, and overpotentials were calculated to predict the catalytic activities for OER and ORR. The results show that introducing heterogeneous metal sites can break the scaling factor, significantly enhancing the bifunctional catalytic activities. An intrinsic descriptor was found to well describe the catalytic activities and provide a better understanding of the local electrical field effects on catalytic activities. Among all the catalysts studied in this work, ZnCo metal pairs show the preeminent bifunctional catalytic activities. Dual-metal catalysts generally suppress the competing two-electron-transfer reaction (formation of H_2O_2) while facilitating the four-electron-transfer ORR and perform better than single- and tri-metal ones and the best commercial noble metal catalysts (e.g., Pt and RuO_2). The predictions are consistent with the previous experimental results. This work provides a theoretical base for rational design of disperse metal atom catalysts with excellent bifunctional catalytic activities.

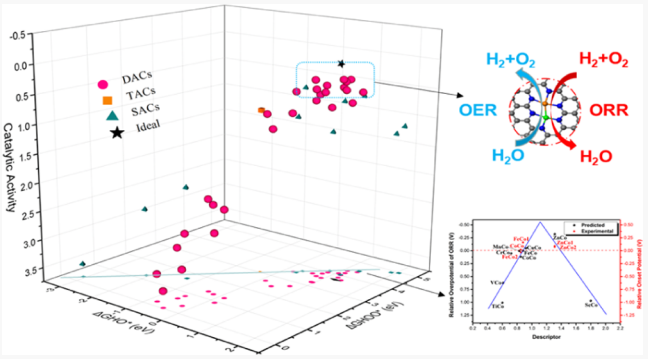

1. INTRODUCTION

With the increasing shortage of energy, the storage and conversion of clean energy have become the focus of scientific research. In the present devices of energy conversion such as fuel cells, metal−air batteries, and water splitting, two main chemical reactions of oxygen reduction reaction (ORR) and oxygen evolution reaction (OER) are sluggish and require catalysts to promote the reactions.[1] Traditionally, precious metal catalysts are commonly used to catalyze the OER and ORR processes (e.g., Pt for ORR[2] and RuO_2 for OER[3]). However, the high cost of precious metals and the scarcity of reserves limit the large-scale commercial use of precious metal catalysts in those devices.[1]

In the past few decades, nonprecious metal or metal-free catalysts have been extensively studied to replace or reduce the use of precious metal-containing catalysts. For metal-free catalysts, nitrogen-doped graphene or carbon nanotubes performed better than noble metals containing catalysts.[4] Additionally, some carbon-based catalysts, including heteroatom-doped graphene, carbon dots, carbon nitride, graphite, and defective graphene, have also been investigated as efficient electrocatalysts.[5−11] However, those electrocatalysts still suffer from sole catalytic activity or other drawbacks in application.[12,13]

Recently, single-atom catalysts (SACs), formed by single metal atoms doped or dispersed on a substrate,[14] attracted much attention because of their lower metal quantity and higher catalytic activity.[12,13,15] In most SACs, two carbon atoms of graphene or other carbon materials were replaced by a metal atom, while four neighboring carbon atoms were substituted by four nitrogen atoms (M-NC).[13−15] Such a structure makes electrons redistribute on the surface of the catalysts, improving the utilization of metal atoms and thus enhancing the catalytic activities. This type of catalysts has been demonstrated to catalyze OER, ORR, hydrogen evolution reaction, and CO_2 reduction reaction (CO_2RR).[13,15−20] However, their functions are limited to sole catalytic activity,

Received: September 24, 2020
Revised: November 22, 2020
Published: December 4, 2020

https://dx.doi.org/10.1021/acs.jpcc.0c08692
J. Phys. Chem. C 2020, 124, 27387−27395

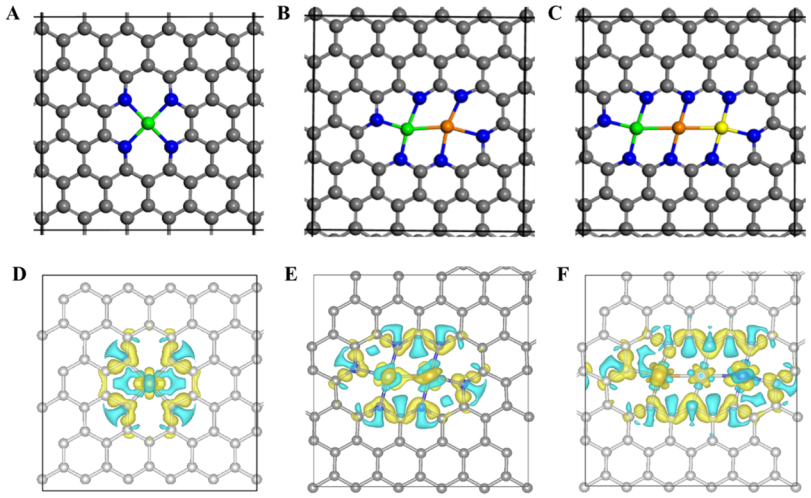

Figure 1. Unit cells of (A) SACs, (B) DACs, and (C) TACs. The black, blue, green, golden, and yellow balls represent the carbon, nitrogen, TM1, TM2, and TM3 atoms, respectively. Optimized structures and differential charge distribution (top view) on (D) SAC, (E) DAC, and (F) FeNiCo-TAC. The blue and yellow colors indicate the positive and negative values of electron quantities, respectively. The isosurface level is 0.01.

either only OER or only ORR. More recently, dual-atom catalysts (DACs), which contain metal pairs coordinated with nitrogen in carbon substrates, have been reported.[21−31] Experiments have shown that the catalytic performance of these DACs is superior to that of SCAs.[28,31] It is expected from the trend that tri-atom catalysts (TACs) would possibly perform even better than SACs or DACs. However, it would be challenging to experimentally screen the best DACs/TACs from numerous combinations of transition metals (TMs).

Recently, computational and theoretical methods have been used to elucidate the microscopic details underlying the mechanisms of operation behind the functions of SACs.[14,15] Activity descriptors have been developed to identify the best ORR/OER catalysts in the SACs, heteroatom-doped carbon nanomaterials, and covalent organic frameworks.[11,15,32] In this study, DACs/TACs will be designed as novel electrocatalysts consisting of two/three 3d TM atoms bonded with each other and each metal is coordinated with nitrogen atoms in graphene. The DFT calculation method will be used to establish a design principle to guide the structural design for DACs/TACs.

2. SIMULATION METHODS

Among nonprecious metals, nickel, cobalt, and iron-doped carbon-based materials performed the best, which are comparable to precious metals.[13,15,31] Based on the reported works, we built three groups of DACs with 3d TM pairs, with BiM-NC (TM-FeNC, TM-CoCN, and TM-NiNC) embedded in the center of graphene (Figure 1B), and based on the formation energies (shown in Table S1), they could exist stably. Such graphene structures with the BiM-NC unit have been synthesized experimentally.[27,30,31] The size of the cells was set to 12.78 Å × 12.30 Å × 20.00 Å. For comparison, similar unit cells were built for the graphene structures with single and three metal cores coordinated with nitrogen, as shown in Figure 1A,C, respectively. The structures were constructed as a three-dimensional periodic structure, where the vacuum layer was set to be around 20 Å in the z-directions to avoid interaction between the slabs.

The free energies and overpotentials of OER and ORR on the structures were calculated with the density functional theory (DFT) method, the Vienna Ab Initio Simulation Package (VASP).[33,34] The Perdew−Burke−Ernzerhof (PBE) exchange correlation functional and soft projector augmented wave pseudopotentials were implemented in the VASP code via the DFT method.[35,36] The PBE functional in our previous studies has been shown to be accurate for the carbon-based system.[37,38] For 3d TMs, DFT + U methods were also considered in the calculations and the values of $U-J$ are listed in Table S2.[39] The cutoff energy of plane wave basis was set at 550 eV, and the structures were sampled by a 3 × 3 × 1 Monkhorst−Pack k-point mesh. Both the cutoff energy and k point meshes were converged within 1 meV in per atom. The van der Waals correction was also taken into consideration in the calculations. The Gaussian smearing method was used to determine the electronic partial occupancies. The whole calculations in spin polarization with the lowest energy magnetic configurations were identified for all the surfaces and the geometries were relaxed until a maximum force of 0.01 eV/Å was converged.

3. RESULTS AND DISCUSSION

3.1. Catalytic Behavior of Disperse Multimetal Catalysts.

3.1.1. Electronic Structures and Reaction Pathways. The electronic structures and Bader effective electron on every metal atom were calculated by DFT methods. Both two- and four-electron-transfer pathways of ORR and OER were analyzed following the reported approaches.[40] Figures 1D−F and S1 show the optimized structures and Bader differential charge density distribution of the structures. From the Bader differential charge density distribution, we could find an interesting phenomenon that nearly all the metal ions are highly positively charged. Because of the synergetic effect of the TM pairs, the metal ions have different amounts of positive charge and the metal center induced by the metal pairs may play a significant role in the catalytic process.[31]

The catalytic activities of the BiM-NC-embedded graphene were evaluated by calculating the minimum overpotentials of ORR and OER on the metal sites. From our previous work,[31] the overpotential η of ORR/OER can be considered as an important measure of the catalytic activities of catalysts. For an ideal OER/ORR catalyst, the overpotential should be zero,

https://dx.doi.org/10.1021/acs.jpcc.0c08692
J. Phys. Chem. C 2020, 124, 27387−27395

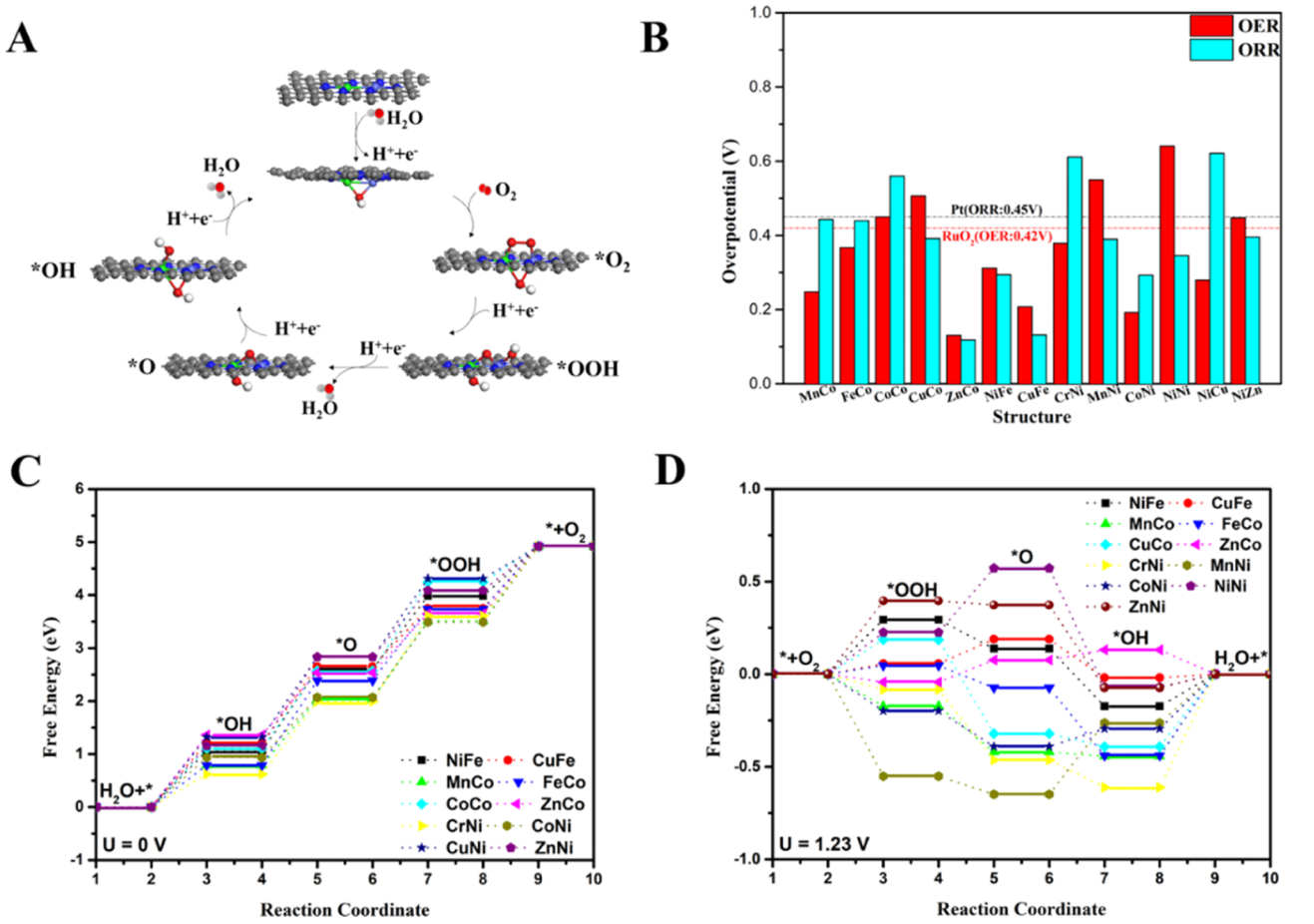

Figure 2. (A) Schematics of ORR cycles on ZnCoNC DAC in four-electron-transfer pathways. The green, purple, blue, gray, red, and white balls refer to Zn, Co, N, C, O, and H, respectively; (B) structures with lower ORR/OER overpotentials compared with noble metal-contained electrocatalysts; free energy diagram of representative DAC structures of (C) OER and (D) ORR in four-electron-transfer pathways when the electrode potentials are 0 and 1.23 V, respectively.

which just promotes the OER/ORR above or very near the equilibrium potential. However, because there are binding energies correlated in the reaction process, the catalysts cannot reach the ideal state. Therefore, the catalyst with lower overpotential shows better catalytic activity.

To find out the lowest overpotentials on the active sites of the DACs, we calculated the free energy of the four elementary steps of OER/ORR on the adsorption sites. Figure S2 shows the free energy diagrams of ORR in four-electron-transfer pathway. In the last electron transfer in ORR, $*OH + H^+ + e^- \rightarrow * + H_2O$, almost all the structures exhibit positive reaction free energies, suggesting that OH* strongly adsorbs on the metal ion and would be difficult to remove during the ORR process.[29,31,41] Therefore, there would be an OH* permanently adsorbed on the metal ions during ORR/OER and the OH* could work as a modifying ligand that influences the catalytic activity. OH as a ligand absorbed on BiM-NC has been demonstrated in our previous work.[31] Although the structures need to be coordinated with an OH ligand, it may link with the metal sites in different ways, such as one of the metal pairs or their bridging ones. Among all the possible structures, it was found that those with OH absorbed on the bridge sites (shown in Figure S3) have the lowest energy and are in the most stable state. Therefore, those modified structures are considered as the initial state of electrocatalysts. While one side of the catalysts is modified by the OH ligand, the other side is exposed to the reaction environment for ORR/OER. In the third electron-transfer pathways of the OER process, the intermediates O* will transfer to HOO*. Because of the modifying ligand OH absorbed on the surface, H is more likely to desorb to form the structures that each side adsorbed one O atom (OO* form). Thus, there will be a competing reaction in this step. We calculated the Gibbs free energy of the two steps, and the results are listed in Table S3. Because the formation of OO* needs to overcome a larger energy barrier, OER on all the structures tends to proceed through the formation of a HOO* intermediate. In the reaction process, the modified ligands may change their adsorption site and configurations during the reaction because of the change of the intermediates on the reaction side, as shown in Figure 2A. The configurations and adsorbing sites during the reactions are summarized in Table S4.

3.1.2. Catalytic Activities. After adding the OH ligand at the sites of the catalysts, we reanalyzed the adsorption energies of the intermediates, $*O_2$, HOO*, O*, and HO*, during ORR and OER. Figures S4 and S5 show the free energy diagrams of OER and ORR on TM-FeNC, TM-CoNC, and TM-NiNC DACs at different electrode potentials, respectively. O_2 molecule is much easier to absorb on the bridge site in a parallel mode compared with other adsorption modes. For most of the BiM-NC structures, the rate-limiting step is the last electron transfer to dissociate the O_2 molecule from the

https://dx.doi.org/10.1021/acs.jpcc.0c08692
J. Phys. Chem. C 2020, 124, 27387−27395

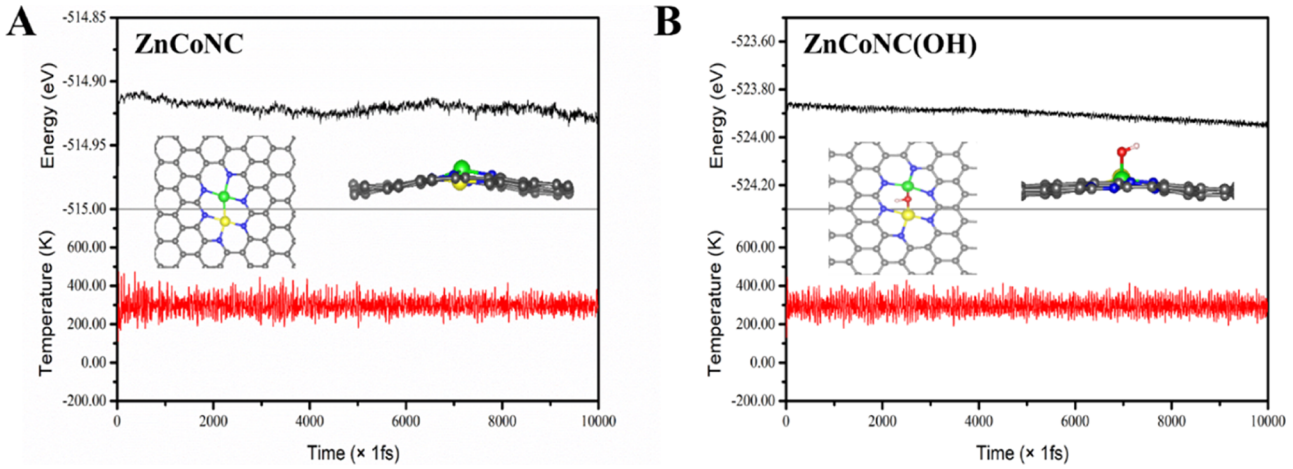

Figure 3. Variations of temperature and energy versus time during AIMD simulations of (A) ZnCoNC and (B) ZnCoNC(OH). The insets show top and side views of the snapshot of the atomic configuration. The simulation was run for 10 ps with a time step of 1 fs at 300 K.

catalytic site (Figures S4 and 2C). Sc-, Ti-, and V-contained structures have very large overpotentials, suggesting that their catalytic activities may be relatively weak (Figure S4). In fact, no work has even been reported on Sc-, Ti-, and V-doped graphene catalysts. Overall, nearly half of the DACs have the OER overpotentials lower than the best OER catalyst, RuO_2, indicating that these DACs may have outstanding catalytic performance (Figure 2B and Table S5). In particular, ZnCoNC DAC has the lowest overpotential (0.13 V) close to the ideal catalysts and may exhibit the excellent OER catalytic activity. Similarly, the rate-limiting step for ORR is also the last electron transfer to form a water molecule (Figures 2D and S5). Most of the DACs have the overpotential lower than the best ORR catalysts, Pt, indicating that they could have better ORR catalytic activity than Pt. Interestingly, ZnCoNC DAC also has the lowest ORR overpotential (0.12 V) among all the structures studied in this work. Additionally, we carried out the ab initio molecular dynamic (AIMD) simulations running at 300 K for 10 ps to evaluate the thermodynamic simulations of ZnCoNC DAC before/after modification of OH ligands. The details of AIMD simulations could be found in Supporting Information.[49] As shown in Figure 3, there is no significant geometrical distortion for ZnCoNC or ZnCoNC-(OH) during the ∼10 ps simulation, indicating relatively high stability of the structure. Therefore, the ZnCoNC DAC could be an excellent bifunctional electrocatalyst for both OER and ORR.

The conductivity of catalysts is one of the important factors that strongly influence the electron transfer in OER/ORR. A high conductivity would enhance the electron transfer and therefore the catalytic activities. We have calculated the density of states (DOS) of those structures that were displayed in Figure 2B. It could be found from the DOS (Figure S6) that the band gaps of those structures near the Fermi level are zero and the designed catalysts may exhibit good conductivity, facilitating the catalytic activities.

For ORR, there is a competing side reaction, two-electron-transfer pathway with the final product of H_2O_2. We have investigated the formation and calculated the free energy and overpotential. Our results show that DACs may suppress this side reaction because of the existence of dual metal pair. In the first elementary step of ORR, the O_2 molecule is adsorbed on two metal sites in the bridging (side-on) mode instead of the end-on mode in SACs. The O−O bond is extended because of the synergistic effect of the metal pair. This leads to the O−O bond to break and form two O* at the metal sites in the following elementary step. Therefore, there is little chance for O_2 to form *OOH on DACs because the DACs are energetically favorable to the dissociate mode (*O and *OH associate on the different metal atom) instead of the associated one (*OOH adsorbed on one metal site in the form of side-on mode) toward H_2O_2. We have compared the overpotentials for two-electron transfer with those of four-electron transfer (Tables S5 and S6); most of the DACs have relatively larger overpotential for two-electron transfer, and consequently, four-electron transfer will dominate the reactions. Although NiCuNC DAC could follow the two-electron-transfer pathway because of its relatively low overpotential (0.21 V for two-electron and 0.26 V for four-electron), this value is still much higher than 0.08 V (Pd catalysts).[42] Therefore, this catalyst could not perform well in facilitating the two-electron pathway to form H_2O_2.

3.1.3. Iron, Cobalt, and Nickel Tri-doped Electrocatalysts. Because the combinations of Fe, Co, and Ni in graphene-based structures are among the best catalysts for ORR/OER, we designed graphene structures with three metal cores (Fe, Co, and Ni) coordinated with nitrogen. Based on the DAC structures and Ye's experimental work,[28] two modeling structures, in-plane and out-plane, might exist. For these two structures, there should be six combination structures of every group; we only chose the most stable one with the lowest formation energy (Table S7) of the in-plane structures, as shown in Figure 1C with the doping order from right to left being Fe, Ni, and Co, respectively.

In ORR/OER on TACs, there are more than two active sites to adsorb intermediates, and the most stable adsorption active site with lowest free energy was chosen as the catalytic active sites. The whole catalytic cycles for four-electron-transfer ORR and OER are more like the SACs, having the last electron transfer as the rate-limiting step. However, the overpotentials of the in-plane structures (OER: 0.75V, and ORR: 0.92V) are higher than that of DACs and noble metal-contained catalysts. For two-electron-transfer ORR, the overpotential is 1.0 V, much higher than that of DACs. The calculation details of two- and four-electron-transfer pathways are listed in Table S7. These results suggest that more metal sites in the catalysts

https://dx.doi.org/10.1021/acs.jpcc.0c08692
J. Phys. Chem. C 2020, 124, 27387−27395

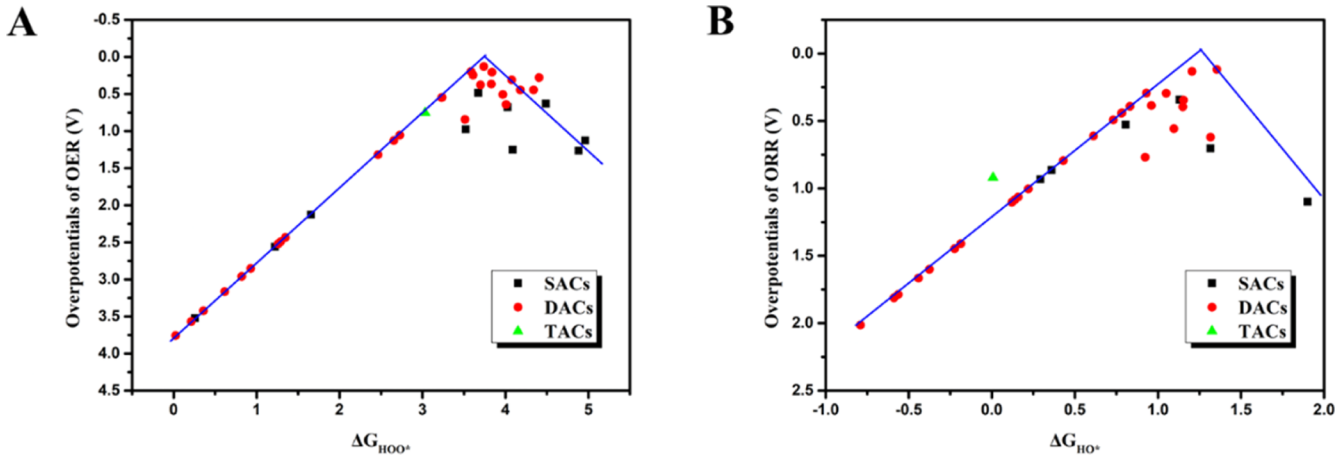

Figure 4. (A) Overpotentials of OER vs the adsorption energy of OOH* and (B) overpotentials of ORR vs adsorption energy of HO* on SACs, DACs, and TACs.

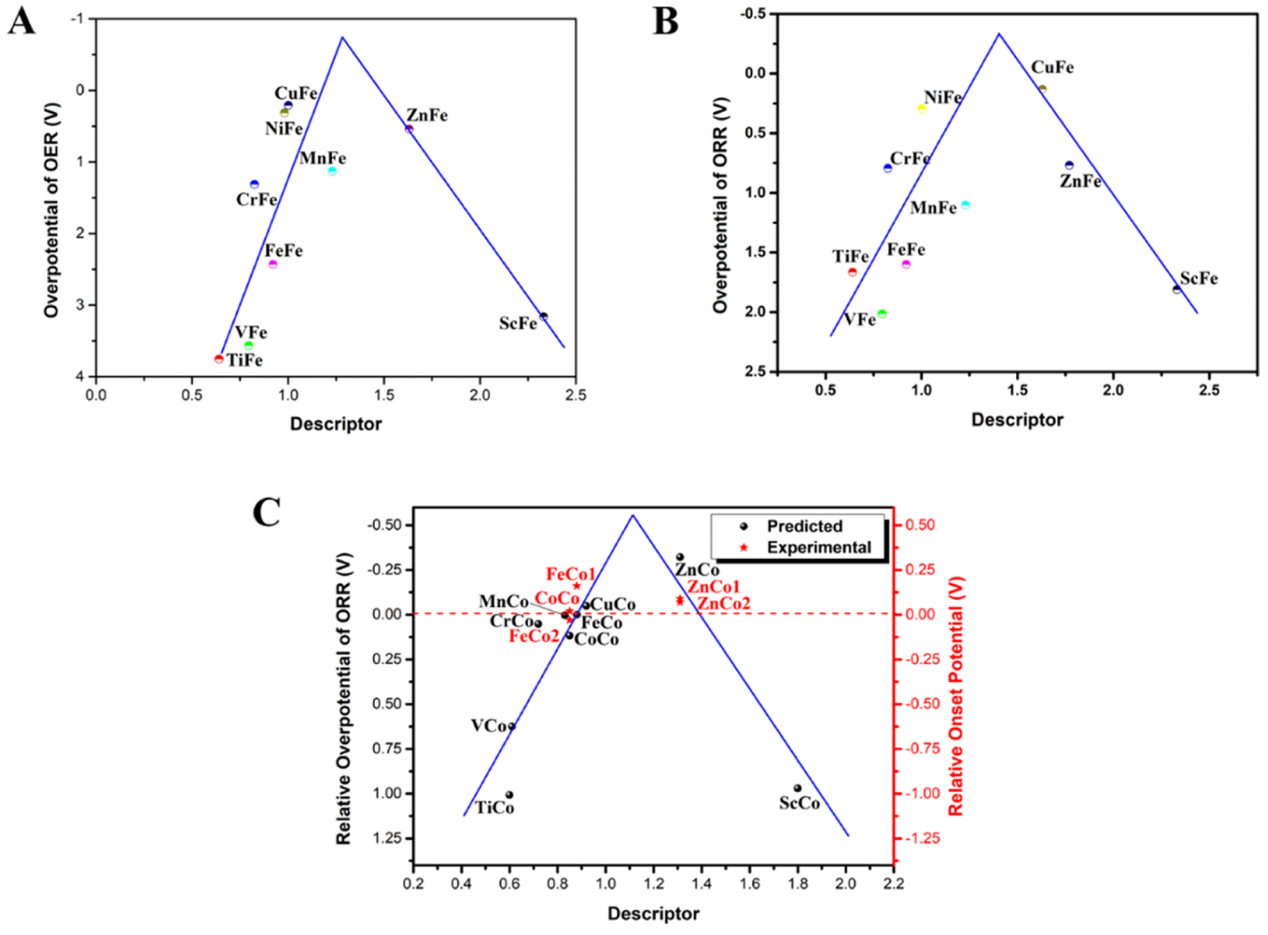

Figure 5. Intrinsic descriptor vs the overpotentials of (A) OER on TM-FeNC DACs and (B) ORR on TM-FeNC DACs. (C) Predicted relative ORR overpotential and measured relative onset potential on TM-CoNC DACs.[24,27,30,31]

would lead to stronger interactions between the intermediates and active sites, which results in difficult dissociation of intermediates from the active sites in the next electron transfer. Although the combination of other TMs would lead to better interactions between the intermediates and active sites, the general trend seems the same.

3.2. Intrinsic Descriptors for Volcano Relationship. To screen excellent electrocatalysts from numerous candidate materials, it is necessary to find descriptors that well describe the catalytic activities of the catalysts. ΔG_{HOO*} and ΔG_{HO*} are considered as effective descriptors to describe the OER and ORR catalytic activities, respectively. Figure 4A,B shows the overpotentials η^{OER} and η^{ORR} versus the descriptors, ΔG_{HOO*} and ΔG_{HO*}, respectively, for SACs, DACs, and TACs. The overpotential shows volcanic relationships with the descriptors for SACs, DACs, and TACs, but the summit of DACs seems not as clear as that of SACs. Overall, the OER and ORR overpotentials of DACs at the summit area are much lower

https://dx.doi.org/10.1021/acs.jpcc.0c08692
J. Phys. Chem. C 2020, 124, 27387−27395

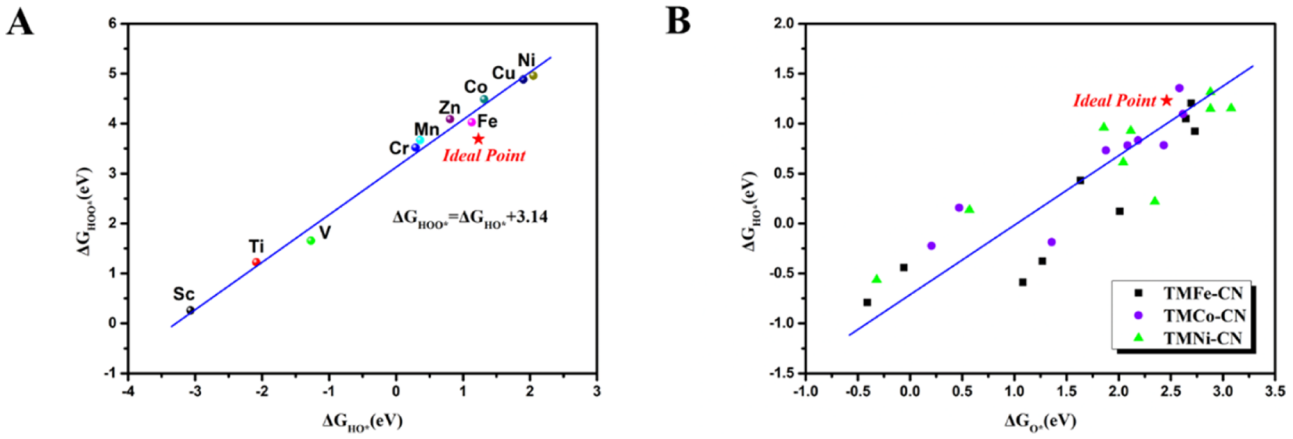

Figure 6. Scaling relations of SACs and DACs: (A) adsorption energy of *OOH vs HO* on SACs and (B) adsorption energy of *OH vs O* on DACs in electron-electron-transfer pathways.

than those of SACs and even lower than noble metal-contained catalysts. The ZnCoNC DAC stands out as one of the best bifunctional catalysts among the DACs studied in this work. Other structures, such as NiFeNC, CoFeNC, MnCoNC, FeCoNC, CoNiNC, and ZnNiNC DACs, are expected to have higher catalytic activities than the Pt-contained catalysts (shown in Figure 4B and Table S5) because of their quite low overpotential. This prediction is supported by our previous experiment that NiFeNC DAC showed excellent bifunctional catalytic activities.[31] For Co-contained DACs, they are more likely to be bifunctional electrocatalysts. In Sun's work, they demonstrated that ZnCoNC exhibits the ORR catalytic activity with an onset potential of 0.97 V in acid media.[30] In alkaline media, Hu's work showed that CoNiNC exhibited outstanding OER and ORR catalytic activity with an onset potential of 0.88 V.[24] More importantly, Dai's group synthesized the CoFeNC catalyst that exhibited excellent ORR activity and stability in both alkaline and acid media.[27]

Although the above descriptor can well predict the catalytic activities of the SACs, DACs, and TACs, it is highly desirable to find out an intrinsic descriptor that is correlated with the catalytic activities such that the best catalysts could be predicted directly from the structures and properties of the catalysts. In the past decades, researchers have found several descriptors to describe the OER and ORR catalytic activity of the different catalysts.[15,32,38] For metal surfaces, the d-band center explains the activity of the TM catalyst.[43,44] In our previous work, we showed that embedded TMs carry different charges in different structures because of the interactions of different elements.[38] For example, an embedded iron atom with strongly positive charge could induce the interfacial electric field, which significantly influences the adsorption of intermediates and thus ORR/OER occurring on the surface of the catalysts. Because the metal center of the DACs was induced by two metal atoms, the electrostatic force might be a good descriptor to describe the activities of the bimetal active sites. Figure S7 shows the effective Bader charge on metal atoms of all the structures. Because dual metal pairs carry more positive charge than the single metal atom, the interaction between intermediates and metal sites may be stronger in DACs than in SACs. According to Coulomb's law, the electrostatic interaction force (F) between the metal center and intermediates may be related to the charge that the TM carries (Q) and the length of the metal−metal pair bond (l). However, the valence electrons of different TMs have significant influence on the physicochemical property of the materials, and we therefore also take the number of valence electrons (k) into consideration. Hence, the new descriptor is defined as

$$F = k\frac{Q_1 Q_2}{l^2}$$

The overpotentials were plotted as a function of the new descriptor in Figures 5 and S8 and the data can be found in Table S8. There is a volcanic relationship between F and the overpotentials. The best catalysts can be identified at the summit or the summit area of the volcano plots. By using this descriptor, the structures such as NiFeNC, CoFeNC, MnCoNC, FeCoNC, CoNiNC, and NiZnNC DACs can be identified to be the superior bifunctional catalytic performance.

The above volcanic relationship is confirmed with the experimental results cited from the literatures. It is well known that the onset potential V_{onset} is a critical indicator of the ORR and OER catalytic activities of the electrocatalysts in fuel cells, metal−air batteries, and water splitting system, and it can be measured by the linear scan voltammogram method. We have compared the predictions with the experimental results of TMCoNC. To make a reliable comparison, the relative onset potential V_{onset} is used, which is defined as the onset potential of the benchmarked Pt/C electrode subtracted by that of the DACs, measured under the same conditions in the same experiment. Similarly, the relative ORR overpotential is calculated by subtracting the overpotential of Pt. Figure 5C shows the relative ORR overpotential predicted by the DFT calculations and the experimental onset potentials of Co-contained DACs. The predictions are consistent with the experiments among the DACs (Table S9).

3.3. Breaking the Scaling Factor with Metal Pairs. Our calculations demonstrate that DACs have much lower overpotential and thus higher catalytic activity than SACs, as shown in Figure 4B,C. This prediction is supported by the experimental results.[24,27,30,31] We have cited the experimental data reported so far for DACs and made a plot of the onset potential of ORR versus the descriptor (Figure 5C). In spite of data scattering due to different measuring conditions, the experimental results are in good agreement with the predictions. This demonstrates the predictive power of the

https://dx.doi.org/10.1021/acs.jpcc.0c08692
J. Phys. Chem. C 2020, 124, 27387−27395

descriptor for guiding the rational design of highly efficient DACs for ORR and OER.

The high catalytic activities of DACs relative to SACs may be attributed to their ability to weaken or break the scaling relations in ORR and OER. In principle, catalysts control the rates in chemical reactions by changing the bonding energy of intermediates relative to one another. In ORR/OER, all the intermediates contain oxygen that directly bond active sites, and thus, the adsorption strengths exhibit highly correlated behavior between different adsorbates, known as adsorbate scaling relations: when a catalyst binds one adsorbate more strongly, it tends to bind similar adsorbates more strongly as well. For SACs, we found that there is a universal scaling relationship, $\Delta G_{HOO*} = \Delta G_{HO*} + 3.14$ eV. Similarly, this scaling relation between the binding energy of different intermediates also exists on some metal-doped carbon-based materials[32,37] and low-index surfaces of metals and their alloys.[45,46] Although these scaling relations can be helpful for fast screening for catalyst discovery, the design flexibility in catalysis is largely limited. This limitation can be broken by introducing a second adsorption site, p states, and a proton acceptor group or changing the solvent composition in the experiment.[47,48] Here, the scaling relations can be changed by introducing metal pairs in active centers. As shown in Figure 6A, the bonding energy of OH is highly correlated with that of OOH and O for SACs, but for bimetal sites in DACs, the scaling relationship between the energy of these intermediate adsorbents is significantly weaken or broken because of the different adsorption modes between OOH and OH. Compared with SACs that have end-on adsorption modes, there are end-on and side-on adsorption mechanisms for DACs, which facilitate intermediate adsorption toward the ideal adsorption state (marked in Figure 6B) and improve their catalytic activity of ORR/OER. Additionally, the metal pairs provide flexible coordination environments for each intermediate to individually optimize the adsorption energy in ORR/OER.

4. CONCLUSIONS

We have calculated the free energy and overpotentials of OER and ORR on disperse single-, dual-, and tri-TM atom catalysts (TM = Sc, Ti, V, Cr, Mn, Fe, Co, Ni, Cu, and Zn) and introduced an intrinsic descriptor to describe the catalytic activities of the catalysts. The DACs could break the scaling factor of SACs and significantly enhance the catalytic activities in both OER and ORR. In addition, introducing metal pairs as an active center can suppress the competing two-electron-transfer reaction (formation of H_2O_2) and facilitate the four-electron-transfer ORR. A design principle has been established to describe the relationship between the catalytic activity and the descriptor. Among the three groups of DACs, MnCoNC (η_{OER} = 0.25 V and η_{ORR} = 0.44 V), FeCoNC (η_{OER} = 0.37 V and η_{ORR} = 0.44 V), ZnCoNC (η_{OER} = 0.13 V and η_{ORR} = 0.12 V), NiCoNC (η_{OER} = 0.19 V and η_{ORR} = 0.29 V), NiFeNC (η_{OER} = 0.31 V and η_{ORR} = 0.29 V), and CuFeNC (η_{OER} = 0.21 V and η_{ORR} = 0.13 V) are predicted to be better bifunctional electrocatalysts for both OER and ORR. While CuNiNC and CrNiNC are identified to be excellent electrocatalysts for OER with overpotentials of 0.28 and 0.38 V in four-electron pathways, respectively, CuCoNC, NiNiNC, and ZnNiNC have better ORR activity with overpotentials of 0.39, 0.35, and 0.40 V, respectively. Tri-metal (Fe, Co, and Ni) co-doped structures have relatively high OER and moderate ORR overpotentials (~0.6 V) and can suppress two-electron-transfer reaction because of their strong adsorption. The predictions are consistent with the experimental results. Our results provide an approach for the rational design of bifunctional DACs, which would work effectively in acidic environments.

■ ASSOCIATED CONTENT

Supporting Information

The Supporting Information is available free of charge at https://pubs.acs.org/doi/10.1021/acs.jpcc.0c08692.

Computational methods; formation energies; $U-J$ parameter values; adsorption energies; intermediates; free energies and overpotentials; calculation results; parameter values; experimental onset potential, turnover frequency, and Tafel plots; optimized structures, free energy diagrams, OH-modified BiM-NC structures, DOS, effective Bader charge, and intrinsic descriptor versus overpotentials (PDF)

■ AUTHOR INFORMATION

Corresponding Authors

Lipeng Zhang − *College of Chemical Engineering, Beijing University of Chemical Technology, Beijing 100029, China;* orcid.org/0000-0001-8743-8985; Email: zhanglipeng2011@gmail.com

Zhenhai Xia − *Department of Materials Science and Engineering, University of North Texas, Denton, Texas 76203, United States;* orcid.org/0000-0002-0881-2906; Email: Zhenhai.xia@unt.edu

Authors

Detao Zhang − *College of Chemical Engineering, Beijing University of Chemical Technology, Beijing 100029, China*

Lele Gong − *College of Chemical Engineering, Beijing University of Chemical Technology, Beijing 100029, China*

Jun Ma − *College of Chemical Engineering, Beijing University of Chemical Technology, Beijing 100029, China*

Xiaowei Wang − *Department of Materials Science and Engineering, University of North Texas, Denton, Texas 76203, United States*

Complete contact information is available at: https://pubs.acs.org/10.1021/acs.jpcc.0c08692

Notes

The authors declare no competing financial interest.

■ ACKNOWLEDGMENTS

D.Z., L.G., J.M., and L.Z. thank the National Key Research and Development Program of China (2017YFA0206500), the National Natural Science Foundation of China (51732002), the Distinguished Scientist Program at BUCT (buctylkxj02) for the financial support. Z.X. and X.W. thank U.S. National Science Foundation (1561886 and 1662288) for the support of this research.

■ REFERENCES

(1) Sealy, L.; Worthington, S. *Sealy & Worthington's Cases and Materials in Company Law*; Oxford University Press: Oxford, U.K., 2013.

(2) Nørskov, J. K.; Rossmeisl, J.; Logadottir, A.; Lindqvist, L.; Kitchin, J. R.; Bligaard, T.; Jonsson, H. Origin of the Overpotential for Oxygen Reduction at a Fuel-Cell Cathode. *J. Phys. Chem. B* **2004**, *108*, 17886−17892.

(3) Man, I. C.; Su, H. Y.; Calle-Vallejo, F.; Hansen, H. A.; Martínez, J. I.; Inoglu, N. G.; Kitchin, J.; Jaramillo, T. F.; Nørskov, J. K.; Rossmeisl, J. Universality in Oxygen Evolution Electrocatalysis on Oxide Surfaces. *ChemCatChem* **2011**, *3*, 1159−1165.
(4) Gong, K.; Du, F.; Xia, Z.; Durstock, M.; Dai, L. Nitrogen-Doped Carbon Nanotube Arrays with High Electrocatalytic Activity for Oxygen Reduction. *science* **2009**, *323*, 760−764.
(5) Lv, Q.; Wang, N.; Si, W.; Hou, Z.; Li, X.; Wang, X.; Zhao, F.; Yang, Z.; Zhang, Y.; Huang, C. Pyridinic Nitrogen Exclusively Doped Carbon Materials as Efficient Oxygen Reduction Electrocatalysts for Zn-Air Batteries. *Appl. Catal., B* **2020**, *261*, 118234.
(6) Kong, X.-K.; Chen, C.-L.; Chen, Q.-W. Doped Graphene for Metal-Free Catalysis. *Chem. Soc. Rev.* **2014**, *43*, 2841−2857.
(7) Qu, L.; Liu, Y.; Baek, J.-B.; Dai, L. Nitrogen-Doped Graphene as Efficient Metal-Free Electrocatalyst for Oxygen Reduction in Fuel Cells. *ACS Nano* **2010**, *4*, 1321−1326.
(8) Liu, X.; Dai, L. Carbon-Based Metal-Free Catalysts. *Nat. Rev. Mater.* **2016**, *1*, 16064.
(9) Jiao, Y.; Zheng, Y.; Jaroniec, M.; Qiao, S. Z. Design of Electrocatalysts for Oxygen-and Hydrogen-Involving Energy Conversion Reactions. *Chem. Soc. Rev.* **2015**, *44*, 2060−2086.
(10) Dai, L.; Xue, Y.; Qu, L.; Choi, H. J.; Baek, J. B. Metal-Free Catalysts for Oxygen Reduction Reaction. *Chem. Rev.* **2015**, *115*, 4823−4892.
(11) Zhang, L.; Niu, J.; Dai, L.; Xia, Z. Effect of Microstructure of Nitrogen-Doped Graphene on Oxygen Reduction Activity in Fuel Cells. *Langmuir* **2012**, *28*, 7542−7550.
(12) Yan, X.; Liu, K.; Wang, T.; You, Y.; Liu, J.; Wang, P.; Pan, X.; Wang, G.; Luo, J.; Zhu, J. Atomic Interpretation of High Activity on Transition Metal and Nitrogen-Doped Carbon Nanofibers for Catalyzing Oxygen Reduction. *J. Mater. Chem. A* **2017**, *5*, 3336−3345.
(13) Fei, H.; Dong, J.; Feng, Y.; Allen, C. S.; Wan, C.; Volosskiy, B.; Li, M.; Zhao, Z.; Wang, Y.; Sun, H.; An, P.; Chen, W.; Guo, Z.; Lee, C.; Chen, D.; Shakir, I.; Liu, M.; Hu, T.; Li, Y.; Kirkland, A. I.; Duan, X.; Huang, Y. General Synthesis and Definitive Structural Identification of Mn_4C_4 Single-Atom Catalysts with Tunable Electrocatalytic Activities. *Nat. Catal.* **2018**, *1*, 63−72.
(14) Ji, S.; Chen, Y.; Wang, X.; Zhang, Z.; Wang, D.; Li, Y. Chemical Synthesis of Single Atomic Site Catalysts. *Chem. Rev.* **2020**, *120*, 11900.
(15) Xu, H.; Cheng, D.; Cao, D.; Zeng, X. C. A Universal Principle for a Rational Design of Single-Atom Electrocatalysts. *Nat. Catal.* **2018**, *1*, 339−348.
(16) Sharifi, T.; Gracia-Espino, E.; Chen, A.; Hu, G.; Wågberg, T. Oxygen Reduction Reactions on Single-or Few-Atom Discrete Active Sites for Heterogeneous Catalysis. *Adv. Energy Mater.* **2020**, *10*, 1902084.
(17) Cao, L.; Luo, Q.; Liu, W.; Lin, Y.; Liu, X.; Cao, Y.; Zhang, W.; Wu, Y.; Yang, J.; Yao, T.; Wei, S. Identification of Single-Atom Active Sites in Carbon-Based Cobalt Catalysts During Electrocatalytic Hydrogen Evolution. *Nat. Catal.* **2019**, *2*, 134−141.
(18) Chivers, B. A. Single-Atom Catalysts: Syntheses, Characterization, and Catalytic Evaluation in Selective Oxidation and Hydrogenation Reactions. Ph.D. Dissertation, University of Saskatchewan, 2020.
(19) Möller, T.; Ju, W.; Bagger, A.; Wang, X.; Luo, F.; Ngo Thanh, T.; Varela, A. S.; Rossmeisl, J.; Strasser, P. Efficient CO_2 to CO Electrolysis on Solid Ni-N-C Catalysts at Industrial Current Densities. *Energy Environ. Sci.* **2019**, *12*, 640−647.
(20) Gong, L.; Zhang, D.; Lin, C. Y.; Zhu, Y.; Shen, Y.; Zhang, J.; Han, X.; Zhang, L.; Xia, Z. Catalytic Mechanisms and Design Principles for Single-Atom Catalysts in Highly Efficient CO_2 Conversion. *Adv. Energy Mater.* **2019**, *9*, 1902625.
(21) Sun, Y.; Wang, J.; Liu, Q.; Xia, M.; Tang, Y.; Gao, F.; Hou, Y.; Tse, J.; Zhao, Y. Itinerant Ferromagnetic Half Metallic Cobalt-Iron Couples: Promising Bifunctional Electrocatalysts for ORR and OER. *J. Mater. Chem. A* **2019**, *7*, 27175−27185.
(22) Hunter, M. A.; Fischer, J. M. T. A.; Yuan, Q.; Hankel, M.; Searles, D. J. Evaluating the Catalytic Efficiency of Paired, Single-Atom Catalysts for the Oxygen Reduction Reaction. *ACS Catal.* **2019**, *9*, 7660−7667.
(23) Wang, J.; Ciucci, F. Boosting Bifunctional Oxygen Electrolysis for N-Doped Carbon Via Bimetal Addition. *Small* **2017**, *13*, 1604103.
(24) Han, X.; Ling, X.; Yu, D.; Xie, D.; Li, L.; Peng, S.; Zhong, C.; Zhao, N.; Deng, Y.; Hu, W. Atomically Dispersed Binary Co-Ni Sites in Nitrogen-Doped Hollow Carbon Nanocubes for Reversible Oxygen Reduction and Evolution. *Adv. Mater.* **2019**, *31*, 1905622.
(25) Xiao, M.; Chen, Y.; Zhu, J.; Zhang, H.; Zhao, X.; Gao, L.; Wang, X.; Zhao, J.; Ge, J.; Jiang, Z.; Chen, S.; Liu, C.; Xing, W. Climbing the Apex of the ORR Volcano Plot Via Binuclear Site Construction: Electronic and Geometric Engineering. *J. Am. Chem. Soc.* **2019**, *141*, 17763−17770.
(26) Wang, J.; Huang, Z.; Liu, W.; Chang, C.; Tang, H.; Li, Z.; Chen, W.; Jia, C.; Yao, T.; Wei, S.; Wu, Y.; Li, Y. Design of N-Coordinated Dual-Metal Sites: A Stable and Active Pt-Free Catalyst for Acidic Oxygen Reduction Reaction. *J. Am. Chem. Soc.* **2017**, *139*, 17281−17284.
(27) Zhang, G.; Jia, Y.; Zhang, C.; Xiong, X.; Sun, K.; Chen, R.; Chen, W.; Kuang, Y.; Zheng, L.; Tang, H.; Liu, W.; Liu, J.; Sun, X.; Lin, W.-F.; Dai, H. A General Route Via Formamide Condensation to Prepare Atomically Dispersed Meta-Nitrogen-Carbon Electrocatalysts for Energy Technologies. *Energy Environ. Sci.* **2019**, *12*, 1317−1325.
(28) Ye, W.; Chen, S.; Lin, Y.; Yang, L.; Chen, S.; Zheng, X.; Qi, Z.; Wang, C.; Long, R.; Chen, M.; Zhu, J.; Gao, P.; Song, L.; Jiang, J.; Xiong, Y. Precisely Tuning the Number of Fe Atoms in Clusters on N-Doped Carbon toward Acidic Oxygen Reduction Reaction. *Chem* **2019**, *5*, 2865−2878.
(29) Xiao, M.; Zhang, H.; Chen, Y.; Zhu, J.; Gao, L.; Jin, Z.; Ge, J.; Jiang, Z.; Chen, S.; Liu, C.; Xing, W. Identification of Binuclear Co_2N_5 Active Sites for Oxygen Reduction Reaction with More Than One Magnitude Higher Activity Than Single Atom CoN_4 Site. *Nano energy* **2018**, *46*, 396−403.
(30) Lu, Z.; Wang, B.; Hu, Y.; Liu, W.; Zhao, Y.; Yang, R.; Li, Z.; Luo, J.; Chi, B.; Jiang, Z.; Li, M.; Mu, S.; Liao, S.; Zhang, J.; Sun, X. An Isolated Zinc−Cobalt Atomic Pair for Highly Active and Durable Oxygen ReductionAn Isolated Zinc-Cobalt Atomic Pair for Highly Active and Durable Oxygen Reduction. *Angew. Chem., Int. Ed.* **2019**, *131*, 2648−2652.
(31) Zhu, X.; Zhang, D.; Chen, C.-J.; Zhang, Q.; Liu, R.-S.; Xia, Z.; Dai, L.; Amal, R.; Lu, X. Harnessing the Interplay of Fe−Ni Atom Pairs Embedded in Nitrogen-Doped Carbon for Bifunctional Oxygen Electrocatalysis. *Nano Energy* **2020**, *71*, 104597.
(32) Lin, C.-Y.; Zhang, D.; Zhao, Z.; Xia, Z. Covalent Organic Framework Electrocatalysts for Clean Energy Conversion. *Adv. Mater.* **2018**, *30*, 1703646.
(33) Kresse, G.; Furthmüller, J. Efficient Iterative Schemes for Ab Initio Total-Energy Calculations Using a Plane-Wave Basis Set. *Phys. Rev. B: Condens. Matter Mater. Phys.* **1996**, *54*, 11169.
(34) Kresse, G.; Furthmüller, J. Efficiency of Ab-Initio Total Energy Calculations for Metals and Semiconductors Using a Plane-Wave Basis Set. *Comput. Mater. Sci.* **1996**, *6*, 15−50.
(35) Blöchl, P. E. Projector Augmented-Wave Method. *Phys. Rev. B: Condens. Matter Mater. Phys.* **1994**, *50*, 17953.
(36) Perdew, J. P.; Burke, K.; Ernzerhof, M. Generalized Gradient Approximation Made Simple. *Phys. Rev. Lett.* **1996**, *77*, 3865.
(37) Lin, C.-Y.; Zhang, L.; Zhao, Z.; Xia, Z. Design Principles for Covalent Organic Frameworks as Efficient Electrocatalysts in Clean Energy Conversion and Green Oxidizer Production. *Adv. Mater.* **2017**, *29*, 1606635.
(38) Zhang, D.; Zhang, J.; Gong, L.; Zhu, Y.; Zhang, L.; Xia, Z. Graphene-Covered Transition Metal Halide Molecules as Efficient and Durable Electrocatalysts for Oxygen Reduction and Evolution Reactions. *Phys. Chem. Chem. Phys.* **2019**, *21*, 23094−23101.
(39) Solovyev, I. V.; Dederichs, P. H.; Anisimov, V. I. Corrected Atomic Limit in the Local-Density Approximation and the Electronic Structure of D Impurities in Rb. *Phys. Rev. B: Condens. Matter Mater. Phys.* **1994**, *50*, 16861.

https://dx.doi.org/10.1021/acs.jpcc.0c08692
J. Phys. Chem. C 2020, 124, 27387−27395

(40) Li, M.; Zhang, L.; Xu, Q.; Niu, J.; Xia, Z. N-Doped Graphene as Catalysts for Oxygen Reduction and Oxygen Evolution Reactions: Theoretical Considerations. *J. Catal.* **2014**, *314*, 66−72.
(41) Holby, E. F.; Taylor, C. D. Activity of N-Coordinated Multi-Metal-Atom Active Site Structures for Pt-Free Oxygen Reduction Reaction Catalysis: Role of *OH Ligands. *Sci. Rep.* **2015**, *5*, 9286.
(42) Verdaguer-Casadevall, A.; Deiana, D.; Karamad, M.; Siahrostami, S.; Malacrida, P.; Hansen, T. W.; Rossmeisl, J.; Chorkendorff, I.; Stephens, I. E. L. Trends in the Electrochemical Synthesis of H_2O_2: Enhancing Activity and Selectivity by Electrocatalytic Site Engineering. *Nano Lett.* **2014**, *14*, 1603−1608.
(43) Hammer, B.; Norskov, J. K. Why Gold Is the Noblest of All the Metals. *Nature* **1995**, *376*, 238−240.
(44) Ruban, A.; Hammer, B.; Stoltze, P.; Skriver, H. L.; Nørskov, J. K. Surface Electronic Structure and Reactivity of Transition and Noble Metals. *J. Mol. Catal. A: Chem.* **1997**, *115*, 421−429.
(45) Seh, Z. W.; Kibsgaard, J.; Dickens, C. F.; Chorkendorff, I.; Nørskov, J. K.; Jaramillo, T. F. Combining Theory and Experiment in Electrocatalysis: Insights into Materials Design. *Science* **2017**, *355*, No. eaad4998.
(46) Deshpande, S.; Kitchin, J. R.; Viswanathan, V. Quantifying Uncertainty in Activity Volcano Relationships for Oxygen Reduction Reaction. *ACS Catal.* **2016**, *6*, 5251−5259.
(47) Huang, Z.-F.; Song, J.; Dou, S.; Li, X.; Wang, J.; Wang, X. Strategies to Break the Scaling Relation toward Enhanced Oxygen Electrocatalysis. *Matter* **2019**, *1*, 1494−1518.
(48) Zhao, Z.-J.; Liu, S.; Zha, S.; Cheng, D.; Studt, F.; Henkelman, G.; Gong, J. Theory-Guided Design of Catalytic Materials Using Scaling Relationships and Reactivity Descriptors. *Nat. Rev. Mater.* **2019**, *4*, 792−804.
(49) Zheng, X.; Yao, Y.; Wang, Y.; Liu, Y. Tuning the electronic structure of transition metals embedded in nitrogen-doped graphene for electrocatalytic nitrogen reduction: a first-principles study. *Nanoscale* **2020**, *12*, 9696−9707.

https://dx.doi.org/10.1021/acs.jpcc.0c08692
J. Phys. Chem. C 2020, 124, 27387−27395